

Gadolinium Complex of 1,4,7,10-Tetraazacyclododecane-*N,N',N'',N'''*-1,4,7-trisacetic Acid (DO3A) Conjugate of Tranexamates: A Quest for a Liver-specific Magnetic Resonance Imaging Contrast Agent

Ki-Soo Nam, Hyun-Jeong Jeong, Hee-Kyung Kim, Garam Choi, Kyung-Jin Suh,[‡]
Yongmin Chang,^{†,§,*} and Tae-Jeong Kim^{*}

Department of Applied Chemistry, Kyungpook National University, Daegu 702-701, Korea. *E-mail: tjkim@knu.ac.kr

[†]Department of Medical & Biological Engineering, Kyungpook National University, Daegu 702-701, Korea

*E-mail: ychang@knu.ac.kr

[‡]Department of Radiology, College of Medicine, Dongguk University, Kyungju 780-714, Korea

[§]Department of Diagnostic Radiology & Molecular Medicine, Daegu 702-701, Korea

Received August 31, 2013, Accepted October 15, 2013

The work is directed toward the synthesis of a series of DO3A conjugates of tranexamates (**1c-e**) and their Gd complexes (**2c-e**) for use as a liver-specific MRI CA. All these complexes show thermodynamic and kinetic stabilities comparable to those of structurally related clinical agents such as Dotarem[®]. Their R_1 relaxivities also compare well with those of commercial agent, ranging 3.68–4.84 mM⁻¹s⁻¹. *In vivo* MR images of mice with **2a-e** reveal that only **2a** exhibits liver-specificity. Although **2b** and **2c** show strong enhancement in liver, yet no bile-excretion is observed to be termed as a liver-specific agent. The rest behaves much like ordinary ECF CAs like Dotarem[®]. The new series possess no toxicity to be employed *in vivo*.

Key Words : MRI, Liver-specific contrast agents, Gadolinium, DO3A, Tranexamate

Introduction

Magnetic resonance imaging (MRI) has been one of the most powerful techniques for the non-invasive diagnostic technique of the human anatomy, physiology and pathophysiology on the basis of superior spatial resolution and contrast.¹ At present, a large number of MRI techniques are performed employing Gd(III) complexes to enhance the image contrast by increasing the water proton relaxation rate in the body. Some representative advantages of employing the Gd(III) ion come from their unique properties such as high magnetic moment and long electron spin relaxation time.² Despite their wide and successful applications in clinics, however, conventional Gd(III)-based contrast agents (GBCAs) are mostly extracellular fluid (ECF) agents exhibiting rapid renal excretion.³⁻⁵ There thus arises the need for new MRI CAs with improved performances and at the same time with special functionality. Much effort has recently been made in an attempt to develop new classes of MRI CAs for use as organ targeting MRI CAs.^{6,7}

Liver-specific CAs for MRI can be divided into two categories: (i) hepatobiliary-specific (or hepatobiliary) agents; (ii) reticuloendothelial cell-specific (or nanoparticulate) agents.^{8,9} The former class of CAs is taken up by functioning hepatocytes and excreted into the bile, and their paramagnetic properties cause shortening of the longitudinal relaxation time (T_1) of the liver and biliary tree.⁶ Currently available CAs of this class are based on Gd-chelates such as Gd-EOB-DTPA (Primovist[®]) and Gd-BOPTA (Multihance[®]) (cf. Chart S1, Supporting Information). On injection, they

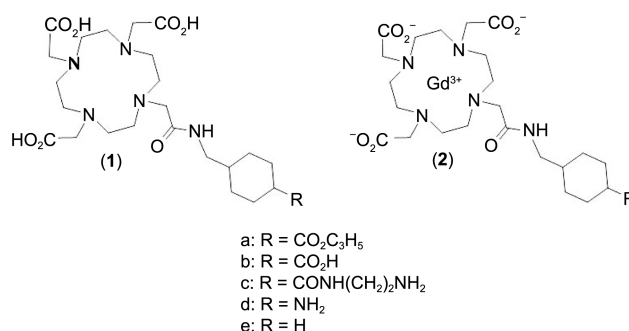


Chart 1

are initially distributed in the ECF CAs compartment and subsequently taken up by hepatocytes.^{10,11} The latter class, on the other hand, targets the Kupffer cells of the reticuloendothelial system, where phagocytosis for CAs occur and, by the effects of iron ions, liver signal intensity decreases giving rise to a “black” liver, instead of “white” one as typically observed with hepatocyte-specific CAs.¹²

We have recently reported the synthesis of some gadolinium complexes of DO3A-tranexamates (**2a-b**, Chart 1) to find that they exhibit a hepatobiliary-specific nature.¹³ Intrigued by these observations and motivated by the recent research activities in an effort to develop multifunctional MRI CAs, we have prepared some more of DO3A-tranexamates such as (**1c-e**) and the corresponding Gd-complexes (**2c-e**) for use as a new class of liver-specific CAs. At the same time we have carried out studies on the structure activity relationship (SAR) for liver-specificity.

Experimental

General Remarks. All reactions were carried out under an atmosphere of dinitrogen using the standard Schlenk techniques. Solvents were purified and dried using standard procedures. 1,4,7,10-Tetraazacyclododecane (DOTA) was purchased from Strem (U.S.) and *trans*-4-(aminomethyl)cyclohexanecarboxylic acid (tranexamic acid) and *trans*-1,4-diaminocyclohexane were obtained from Aldrich and aminomethylcyclohexane was obtained from TCI. All other commercial reagents were purchased from Aldrich and used as received unless otherwise stated. Deionized (DI) water was used for all experiments. The ^1H experiments were performed on a Bruker Advance 400 or 500 spectrometer at KBSI. Chemical shifts were given as δ values with reference to tetramethylsilane (TMS) as an internal standard. Coupling constants are in Hz. FAB mass spectra were obtained by using a JMS-700 model (Jeol, Japan) mass spectrophotometer. MALDI-TOF mass spectra were obtained by using a Voyager DE-STR (Applied biosystems, U.S.). Elemental analyses were performed by Center for Scientific Instruments, KNU.

Synthesis of Ligand. 1a and 1b were prepared according to the literature method.¹³

1c: To neat 1,2-diaminoethane (2.3 mL, 33.8 mmol) was added DO3A(*t*Bu)₃ conjugate of tranexamic ethyl ester (6.8 mmol) prepared following the literature method (cf, R = CO₂Et, Chart 1).¹³ The mixture was stirred at RT for 72 h after which chloroform was added to be extracted with water (30 mL \times 3 times). The organic extract was dried over MgSO₄, filtered, and evaporated to give a crude product which was further purified by chromatography on silica (gradient elution CH₂Cl₂ to 10% MeOH-CH₂Cl₂, R_f = 0.6 (MeOH/CH₂Cl₂ = 2:8)) to give a yellow solid. This was dissolved in dichloromethane (10 mL) and trifluoroacetic acid added for deprotection of *tert*-buthyl groups. The mixture was stirred overnight at RT and the solvent removed under vacuum to leave an oily residue which was taken up in water. Acetone was added to precipitate the product as a white solid which was washed with acetone a few times and dried under vacuum: Yield: 0.36 g (92%). ^1H NMR (D₂O) δ 3.82 (s, 4H, -NCH₂CO₂-), 3.62 (2H, -NCH₂CO₂-), 3.67 (s, 2H, -CH₂CON), 3.44 (m, 10H, overlapped -NCH₂CH₂N- in the ring (8H) & -CONHCH₂- (2H)), 3.08 (d, 2H, -CONHCH₂C-), 2.24/1.52 (m, 2H, -CONH), 1.85/1.41 (m, 8H, -CH₂-, cyclohexyl), 1.03 (m, 2H, -CH₂-, cyclohexyl). Anal. Calcd for C₂₆H₄₇N₇O₈·2H₂O: C, 50.23; H, 8.27; N, 15.77. Found: C, 50.66; H, 8.24; N, 16.01. MALDI-TOF MS (m/z): Calcd for C₂₆H₄₇N₇O₈: 585.35, Found: 586.74 ([MH]⁺), 608.70 ([MNa]⁺).

1d: To a solution of *trans*-[4-(2-chloroacetylamino)cyclohexyl]carbamic *tert*-butyl ester (1.0 g, 3.4 mmol) in chloroform (100 mL) prepared from *trans*-1,4-cyclohexane according to the literature methods^{14,15} was added DO3A-(*t*BuO)₃ (1.6 g, 3.1 mmol). The mixture was stirred at RT for 24 h, any solids removed by filtration, and the filtrate evaporated under vacuum to leave a yellowish oily residue. Column chromatography on silica (gradient elution : CH₂Cl₂ to 10%

MeOH-CH₂Cl₂, R_f = 0.4 (MeOH/CH₂Cl₂ = 1:9)) followed by usual workups gave an off-white solid. This was re-dissolved in dichloromethane to which was added an excess amount of TFA. Stirring was continued overnight after which methanol was added to precipitate out a white solid which was further purified by usual workups. Yield: 0.62 g (87%). ^1H NMR (D₂O) δ 3.72 (m, 10H, overlapped -NCH₂CO₂- (8H), -CONHCH- & H₂NCH- (2H)), 3.40/3.21 (m, 16H, -NCH₂-CH₂N-), 2.06/1.55/1.38 (m, 8H, -CH₂-, cyclohexyl). Anal. Calcd for C₂₂H₄₀N₆O₇·2CF₃COOH·2H₂O: C, 39.00; H, 6.29; N, 10.50. Found C, 39.13; H, 6.05; N, 9.35. MALDI-TOF MS (m/z): Calcd for C₂₂H₄₀N₆O₇: 500.30, Found: 501.33 [MH]⁺, 523.33[MNa]⁺.

1e: To a solution of 2-chloro-*N*-cyclohexylmethylacetamide (1.2 g, 6.4 mmol) in acetonitrile (30 mL) prepared according to the literature method¹⁶ was added DO3A-(*t*BuO)₃ (3.0 g, 5.8 mmol). The solution was stirred at RT for 24 h. Solid impurities were removed by filtration and the filtrate evaporated under vacuum to give an oily residue. Column chromatography on silica (gradient elution : CH₂Cl₂ to 10% MeOH-CH₂Cl₂, R_f = 0.4 (MeOH/CH₂Cl₂ = 1:9)) followed by evaporation under a reduced pressure yielded an off-white solid. Deprotection by TFA followed by usual workups as described above for the preparation of **1d** yielded the product as an off-white solid. Yield: 2.4 g (82%). ^1H NMR (D₂O) δ 3.74/3.57 (m, 8H, -NCH₂CO₂-), 3.30 (m, 10H, overlapped -NCH₂CH₂N- (8H) & -CONHCH₂- (2H)), 3.10 (m, 8H, -NCH₂CH₂N-), 1.98/1.44/1.27 (m, 4H, -CH₂-, cyclohexyl), 1.88 (m, 1H, -NHCH₂CH-). Anal. Calcd for C₂₂H₃₉N₅O₇·3CF₃COOH·3H₂O: C, 38.14; H, 5.49; N, 7.94. Found: C, 37.83; H, 5.76; N, 8.44. MALDI-TOF MS (m/z): Calcd for C₂₂H₃₉N₅O₇: 485.28, Found: 486.42 ([MH]⁺), 508.44 ([MNa]⁺).

Synthesis of Gd Complex. 2a and 2b were prepared according to the literature method.¹³

2c: To a solution of **1c** (1.0 g, 1.7 mmol) in water (50 mL) was added gadolinium chloride (0.64 g, 1.7 mmol) and the mixture was stirred at 50 °C for 48 h. The pH was periodically checked and adjusted to 7.0-7.5 using 1 N NaOH. The reaction mixture was dried under vacuum to leave an oily residue which was taken up in water. Acetone was added to the solution to precipitate a white solid which was separated by filtration, washed with acetone, and dried under vacuum. The product was obtained as a hygroscopic ivory solid. Yield: 0.75 g (86%). Anal. Calcd for C₂₆H₄₄GdN₇O₈·2CF₃COOH·8H₂O: C, 32.40; H, 5.62; N, 8.82. Found: C, 31.99; H, 5.22; N, 9.00. HR-FABMS (m/z): Calcd for C₂₆H₄₅GdN₇O₈, 741.26 ([MH - H₂O]⁺). Found: 741.2567; Calcd for C₂₆H₄₄-GdN₇O₈Na, 763.24 ([MNa - H₂O]⁺). Found: 763.2397.

2d: The title compound was prepared in the same manner as above by replacing **1c** with **1d**. The product was obtained as an off-white, hygroscopic solid. Yield: 1.15 g (88%). Anal. Calcd for C₂₂H₃₇GdN₆O₇·2CF₃COOH·5H₂O: C, 32.10; H, 5.08; N, 8.64. Found: C, 31.55; H, 5.09; N, 9.06. HR-FABMS (m/z): Calcd for C₂₂H₃₈GdN₆O₇, 656.21 ([MH - H₂O]⁺). Found: 656.2045; Calcd for C₂₆H₄₄GdN₇O₈Na, 678.19 ([MNa - H₂O]⁺). Found: 678.1867.

2e: The title compound was prepared in the same manner

as above by replacing **1c** with **1e**. The product was obtained as an off-white, hygroscopic solid. Yield: 0.75 g (86%). Anal. Calcd for $C_{23}H_{38}GdN_5O_7 \cdot 4H_2O$: C, 38.06; H, 6.39; N, 9.65. Found: C, 38.59; H, 6.09; N, 9.69. HR-FABMS (m/z): Calcd for $C_{23}H_{39}GdN_5O_7$, 655.21 ($[MH - H_2O]^+$). Found: 655.2093.

Relaxivity. T_1 measurements were carried out using an inversion recovery method with a variable inversion time (TI) at 1.5 T (64 MHz). The MR images were acquired at 35 different TI values ranging from 50 to 1750 ms. T_1 relaxation times were obtained from the nonlinear least-squares fit of the signal intensity measured at each TI value. For T_2 measurements the CPMG (Carr-Purcell-Meiboom-Gill) pulse sequence was adapted for multiple spin-echo measurements. Thirty-four images were acquired with 34 different echo time (TE) values ranging from 10 to 1900 ms. T_2 relaxation times were obtained from the nonlinear least-squares fit of the mean pixel values for the multiple spin-echo measurements at each echo time. Relaxivities (R_1 and R_2) were then calculated as an inverse of relaxation time per mM. The determined relaxation times (T_1 and T_2) and relaxivities (R_1 and R_2) are finally image processed to give the relaxation time map and relaxivity map, respectively.

Transmetalation Kinetics. This experiment was prepared according to the literature method.¹⁷ It is based on measurement of the evolution of the water proton longitudinal relaxation rate (R_1^P) of a buffered solution (phosphate buffer, pH 7.4) containing 2.5 mmol/L gadolinium complex and 2.5 mmol/L $ZnCl_2$. Then 10 μ L of a 250 mmol/L solution of $ZnCl_2$ is added to 1 mL of a buffered solution of the paramagnetic complex. The mixture is vigorously stirred, and 300 μ L is taken up for the relaxometric study. A control study, run on Gd-DOTA, Gd-BOPTA, Gd-DTPA-BMA, and Gd-EOB-DTPA has given results identical to those obtained in the presence of $ZnCl_2$. The R_1^P relaxation rate is obtained after subtraction of the diamagnetic contribution of the proton water relaxation from the observed relaxation rate $R_1 = (1/T_1)$. The measurements were performed on a 3T whole body system (Magnetom Tim Trio, Siemens, Korea Institute of Radiological & Medical Science), at room temperature.

Isothermal Titration Calorimeter (ITC). ITC experiments were performed in VP-ITC isothermal titration microcalorimeter (Microcal, USA) to quantify the binding isotherms of paramagnetic metal ion Gd^{3+} to ligand solutions.¹⁸⁻²⁰ Data collection, analysis and plotting were performed with resort to the software package Origin, version 8.0, supplied by Microcal. The sample cell had a volume of 1.43 mL. It was filled with aqueous buffered solutions of **1a-e** ligands (0.2 mM). An aqueous buffered solution of Gd^{3+} (1.0 mM) was placed in a 300 μ L continuously stirred (300 rpm) syringe and injected into the cell in 10 μ L aliquots, delivered over 20 s in intervals of 3 min. Data points were collected every 2 s. The measurements were performed at 25 °C. All titrations were carried out three times to ensure consistency of the data and stability of the solutions. These titration isotherms were integrated to provide the enthalpy change upon each injection. Isotherms were analyzed to fit well to two mathemati-

cally different sets of site models. Through the calorimetric analysis, parameters including the binding constant (K_a), the change in enthalpy (ΔH), and the stoichiometry of binding (N) were calculated. The changes in free energy (ΔG) and entropy (ΔS) were then determined using the equation for the complexation, $M^{n+} + nL \leftrightarrow ML_n$: $\Delta G = -RT \cdot \ln K_a = \Delta H - T\Delta S$, wherein R is the universal gas constant and T is the temperature in degrees Kelvin.

In vivo MR Experiments. The *in vivo* study was performed in accordance with the rules of the animal research committee of Kyungpook National University. Six-week male ICR mice with weights of 29-31 g were used for the *in vivo* study. The mice (n = 3) were anesthetized by 1.5% isoflurane in oxygen. Measurements were made before and after injection of **2a-e** *via* tail vein. The amount of CAs per each injection is as follows: 0.1 mmol of Gd/kg for MR images. After each measurement the mice were revived from anesthesia and placed in the cage with free access to food and water. During these measurements, the animals were maintained at approximately 37 °C using a warm water blanket. MR images were taken with a 1.5 T MR unit (GE Healthcare, Milwaukee, WI) equipped with a homemade small animal RF coil. The coil was of the receiver type with its inner diameter being 50 mm. The imaging parameters for spin echo (SE) are as follows: repetition time (TR) = 300 msec; echo time (TE) = 13 msec; 8 mm field of view (FOV); 192×128 matrix size; 1.2 mm slice thickness; number of acquisition (NEX) = 8. MR images were obtained for 24 h after injection.

The anatomical locations with enhanced contrast were identified with respect to liver, bile duct, and kidney on post contrast MR images. For quantitative measurement, signal intensities in specific regions of interest (ROI) were measured using Advantage Window software (GE medical, U.S.). The CNR was calculated using Eq. (1), where SNR is the signal-to-noise ratio.

$$CNR = SNR_{post} - SNR_{pre} \quad (1)$$

Cell Viability Assay. Normal conjunctiva fibroblast cells were used. Cells were maintained in DMEM (Gibco®) supplemented with heat-inactivated FCS (10%), penicillin (100 IU/mL), streptomycin (100 mg/mL), and gentamicin (200 mg/mL) (all purchased from Gibco®). The medium was replaced every 2 days, and cells split into a 96-well plate (1×10^4 cells/well/200 μ L). Various Gd(III) concentrations (50-500 μ M) of the contrast agent were added into the culture serum free media and incubated for 24 h. CCK-8 (10 μ L) was then added to each well to evaluate cell viability. The solution was removed after 4 h at 37 °C. The O. D. (Optical Density) read at 450 nm using a microplate reader (Molecular Device, USA Bio-rad 550 Reader) to determine the cell viability/toxicity.

Kinetic Stability in Variable pH Regions. The stability was given in the evolution of the water proton relaxation rate (R_1) for 2 ([Gd] = 1.0 mM) in PBS at different pH conditions (pH: 1, 3, 5, 7, 9 and 11) as a function of incubation time at RT. The measurements were performed on a 1.5 T whole body system (GE Healthcare, Milwaukee, WI, USA).²¹

Results and Discussion

Synthesis. As mentioned above, the search for a new series of liver-specific MRI CAs is motivated by our early findings that **2a** serves as a kinetically inert and biocompatible chelate for Gd complex which reveals in a certain degree liver-specificity as well as HSA targeting.¹³ A new series of DO3A conjugate of tranxamates comprises **2c-e**, and their synthesis is typically based on the synthesis of **2a** with a slight modification. Namely, the synthesis initially begins with the formation of DO3A(*t*-Bu)₃ conjugate of tranxamates followed by deprotection of *tert*-butyl groups by TFA to form the series **1** which in turn yields the series **2** after complexation with gadolinium chloride (cf. Schemes S1-3, Supporting Information). Their synthesis was confirmed by microanalysis and various spectroscopic techniques.

Relaxivity. **2a-e** reveals R_1 relaxivities in PBS comparable well with and for some cases better than those of clinically available MRI CAs such as Gd-DOTA (Dotarem[®]) and Gd-BT-DO3A (Gadovist[®]) (Table 1). When the comparison is made within the series, no observable differences in R_1 's are perceived. Measurements were made in two different media, PBS (pH = 7.4) and a PBS solution of HSA to see whether they show any blood-pool effect. Any significant increase in R_1 is observed in HSA as compared with R_1 's in PBS, indicating there is in fact little interaction between our new series with HSA.

Kinetic Stability. The evaluation of the normalized paramagnetic longitudinal relaxation rates $R_1^P(t)/R_1^P(0)$ were observed with the present series **2a-e** and with Dotarem[®], Primovist[®], Multihance[®], Omniscan[®] for comparative purposes (Figure 1). The complexes put into examination may be classified into two groups depending on the pattern of evolution: (i) those adopting macrocyclic chelates; (ii) those with acyclic chelate. The present series adopt the macrocyclic ring and quite expectedly possess pretty high kinetic inertness to retain more than 90% of the paramagnetic relaxation rate during the initial measurement for 72 h. In contrast, however, a drastic decrease in the rate is observed with those belonging to the latter group. For instance, the slope becomes even steeper with Primovist[®] and Multihance[®] to retain only 50% of the initial relaxation rate during the same period of measurement. The present series exhibit high kinetic stability as well throughout a wide range of pH from 3 to 11 (Figure S1). It is to be noted that **2a** is stable enough

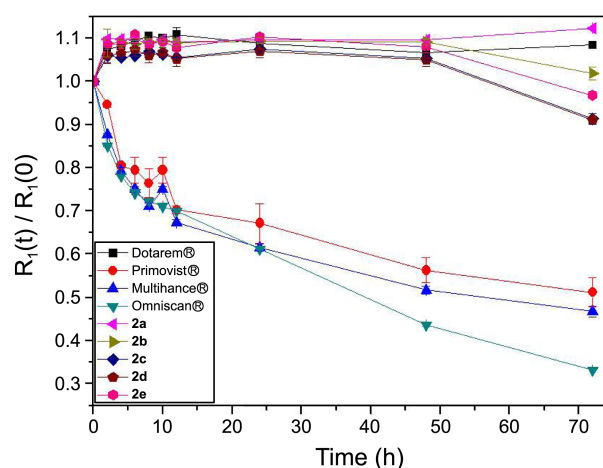


Figure 1. Evolution of $R_1^P(t)/R_1^P(0)$ as a function of time for various MRI CAs.

even at pH 1.

Analyzing Thermodynamic Data. High thermodynamic stabilities of the present series have also to be noted in that they all reveal high formation constants (K_a) with an order of four as measured by isothermal titration calorimetry (Table S1 & Figure S2). When the comparison is made within the series, **1b** shows the highest preference for the Gd^{3+} ion for the reason unknown.

In vivo MRI. Strong signal enhancement both in heart and abdominal aorta is observed within 5 min with **2a-e** (Figure 2(a)). Of the five, the first three (**2a-c**) are comparable with Primovist[®] and Multihance[®], typical liver-specific CAs in that they exhibit enhancement in liver for the initial one hour. Yet, by comparison with Primovist[®] and Multihance[®], only **2a** can be classified as a true liver-specific CA in that it shows excretion through bile (Figure 2(b)). Although **2e** also shows bile-excretion, the signal enhancement is too weak to be termed as a liver-specific CA. The signal intensity with **2e** is as weak as that with Gadovist[®], a typical ECF agent (Figure 2(a)). Although **2d** shows initially strong enhancement both in kidney and abdominal aorta, it is to be classified as a ECF agent as well in that excretion is almost complete within an hour like Gadovist[®]. As for **2b** and **2c**, strong enhancement in liver is also notable (Figures 2(a) & S3), yet no bile-excretion is observed. Two assumptions may be cited to explain such an unusual behavior observed with **2b** and **2c**: Either inability of multidrug resistance protein 2

Table 1. Relaxivity data of **2a-e**, Gd-DOTA and Gd-BT-DO3A in PBS and 0.67 mM HSA (64 MHz, 293 K)

	R_1 ($mM^{-1}s^{-1}$)	R_2 ($mM^{-1}s^{-1}$)	R_1 ($mM^{-1}s^{-1}$) in 0.67 mM HSA	R_2 ($mM^{-1}s^{-1}$) in 0.67 mM HSA
2a	4.84 ± 0.18	4.91 ± 0.25	5.11 ± 0.10	6.04 ± 0.13
2b	3.87 ± 0.11	3.98 ± 0.26	3.98 ± 0.14	5.43 ± 0.28
2c	3.68 ± 0.13	3.62 ± 0.26	3.74 ± 0.07	4.10 ± 0.07
2d	3.94 ± 0.13	3.68 ± 0.29	3.91 ± 0.09	4.07 ± 0.09
2e	4.49 ± 0.18	4.52 ± 0.28	5.21 ± 0.23	6.22 ± 0.28
Dotarem [®]	3.59 ± 0.17	3.87 ± 0.20	4.05 ± 0.13	4.30 ± 0.25
Gadovist [®]	4.38 ± 0.15	4.27 ± 0.30	4.81 ± 0.17	5.54 ± 0.24

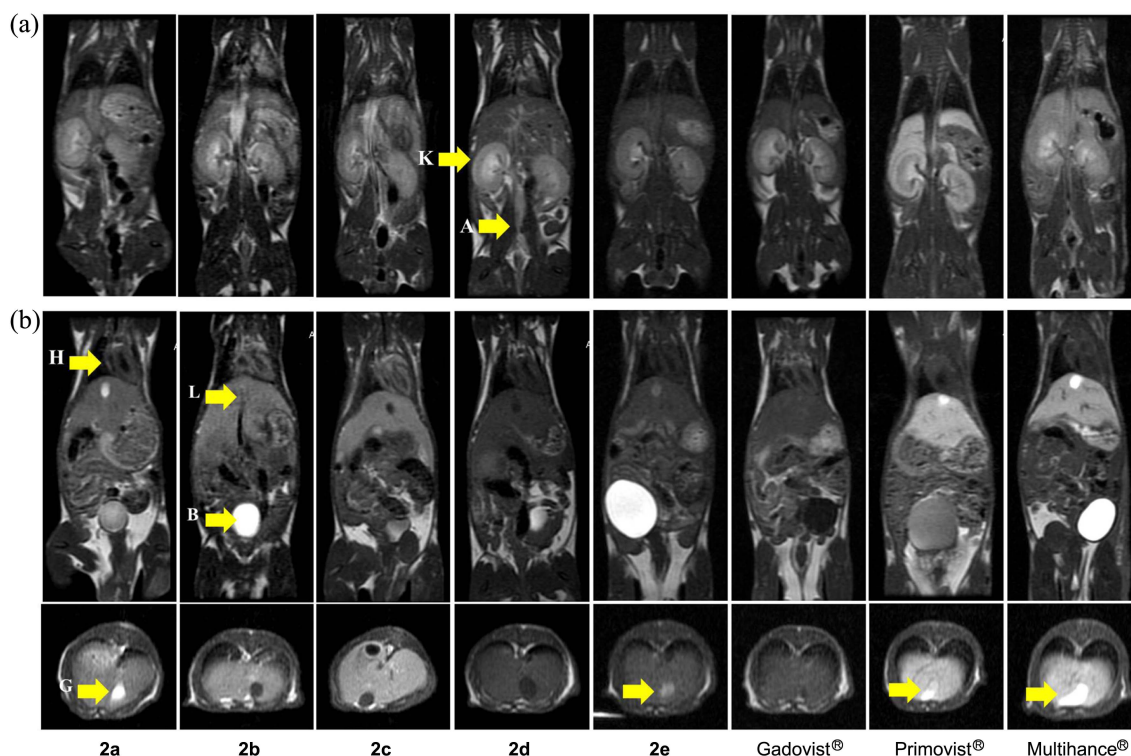


Figure 2. (a) The coronal and axial T_1 -weighted images of ICR mice 5 min after injection with CAs: K, Kidney; A, Abdominal aorta. (b) The coronal and axial T_1 -weighted images of ICR mice 1 h after injection with CAs: H, Heart; L, Liver; B, Bladder; G, Gallbladder.

(MRP2), a transporter molecule present at the canalicular membrane of the cell, to transport **2b** and **2c** after they enter hepatocytes through organic anion transporting polypeptide (OATP); or return of **2b** and **2c** back to sinusoids *via* MRP3 or bidirectional OATP.²² It is to be noted that as for the typical liver-specific agents Primovist[®] and Multihance[®], passive diffusion takes place *via* OATP1 present on the basolateral membrane of the normal hepatocytes. Excretion into bile is followed by the action of MRP2.^{23,24} The presence of lipophilic ethoxybenzyl in Primovist[®] and Multihance[®] is believed to play a key role in all this process. In this regard, the presence of lipophilic cyclohexyl moiety in **2a** may also be playing a similar role. This issue is the subject of future investigation.

Cell Cytotoxicity. Cell viability of **2b-e** compares well with that of Dotarem[®] (Figure 3). Namely, neither cell proliferation and nor the viability is affected when incubated for

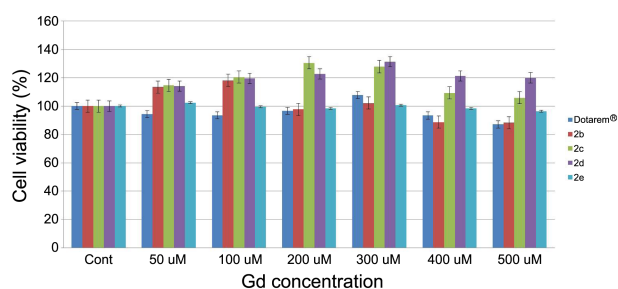


Figure 3. Relative cell cytotoxicity (%) of the normal conjunctiva fibroblast cells obtained by Gd-DOTA and **2b-e**. The standard deviations (\pm SD) were obtained on a triplicate analysis ($n = 3$).

24 h. Little difference is found within the series as well with no sign of cytotoxicity in the concentration range required for obtaining intensity enhancement in the MR images.

Conclusion

A new series of DO3A conjugates of tranxamates (**1c-e**) and their Gd complexes (**2c-e**) were prepared for use as a liver-specific MRI CA. All these complexes show thermodynamic and kinetic stabilities, R_1 relaxivities comparable to those of structurally related clinical agents such as Dotarem[®]. A brief study on the structure activity relationship was carried out to find that of five complexes (**2a-e**), only **2a** reveals liver-specificity. Although **2b** and **2c** show strong enhancement in liver, yet no bile-excretion is observed to be termed as a liver-specific agent. The rest behaves much like ordinary ECF CAs like Dotarem[®]. The new series possess no toxicity to be employed *in vivo*.

Acknowledgments. This work was supported by NRF through the Basic Science Research Program (2010-0024143 and 2011-0015353).

References

- Caravan, P. *Chem. Soc. Rev.* **2006**, 35, 512.
- Caravan, P.; Ellison, J. J.; McMurry, T. J.; Lauffer, R. B. *Chem. Rev.* **1999**, 99, 2293.
- Kobayashi, H.; Sato, N.; Hiraga, A.; Saga, T.; Nakamoto, Y.; Ueda, H.; Konishi, J.; Togashi, K.; Brechbiel, M. W. *Mag. Reson. Med.* **2001**, 45, 454.

4. Ayyagari, A. L.; Zhang, X.; Ghaghada, K. B.; Annapragada, A.; Hu, X.; Bellamkonda, R. V. *Mag. Reson. Med.* **2006**, *55*, 1023.
 5. Schwickert, H. C.; M., S.; van Dijke, C. F.; Roberts, T. P.; Mann, J. S.; Demsar, F.; Brasch, R. C. *Acad. Radiol.* **1995**, *2*, 851.
 6. Seale, M. K.; Catalano, O. A.; Saini, S.; Hahn, P. F.; Sahani, D. V. *Radiographics* **2009**, *29*, 1725.
 7. Schima, W. *Wiener Medizinische Wochenschrift. Supplement* **2002**; p 8.
 8. Gandhi, S. N.; Brown, M. A.; Wong, J. G.; Aguirre, D. A.; Sirlin, C. B. *Radiographics* **2006**, *26*, 1621.
 9. Chanyaputhipong, J.; Low, S. C.; Chow, P. K. *Int. J. Hepatol.* **2011**, *2011*, 489342.
 10. Zizka, J.; Klzo, L.; Ferda, J.; Mrklovsky, M.; Bukac, J. *Eur. J. Radiol.* **2007**, *62*, 186.
 11. Saito, K.; Kotake, F.; Ito, N.; Ozuki, T.; Mikami, R.; Abe, K.; Shimazaki, Y. *Magnetic Resonance in Medical Sciences: MRMS: an Official Journal of Japan Society of Magnetic Resonance in Medicine* **2005**, *4*, 1.
 12. Saini, S.; Stark, D. D.; Hahn, P. F.; Bousquet, J. C.; Introcasso, J.; Wittenberg, J.; Brady, T. J.; Ferrucci, J. T., Jr. *Radiology* **1987**, *162*, 217.
 13. Gu, S.; Kim, H. K.; Lee, G. H.; Kang, B. S.; Chang, Y.; Kim, T. J. *J. Med. Chem.* **2011**, *54*, 143.
 14. Lee, D. W.; Ha, H. J. *Synthetic. Commun.* **2007**, *37*, 737.
 15. Roth, G. J.; Heckel, A.; Colbatzky, F.; Handschuh, S.; Kley, J.; Lehmann-Lintz, T.; Lotz, R.; Tontsch-Grunt, U.; Walter, R.; Hilberg, F. *J. Med. Chem.* **2009**, *52*, 4466.
 16. Cho, S. D.; Song, S. Y.; Kim, K. H.; Zhao, B. X.; Ahn, C.; Joo, W. H.; Yoon, Y. J.; Falck, J. R.; Shin, D. S. *B Kor. Chem. Soc.* **2004**, *25*, 415.
 17. Laurent, S.; Elst, L. V.; Copoix, F.; Muller, R. N. *Investigative radiology* **2001**, *36*, 115.
 18. Gouin, S.; Winnik, F. M. *Bioconj. Chem.* **2001**, *12*, 372.
 19. Pierce, M. M.; Raman, C. S.; Nall, B. T. *Methods* **1999**, *19*, 213.
 20. Velazquez-Campoy, A.; Freire, E. *Nat. Protoc.* **2006**, *1*, 186.
 21. Jung, K. H.; Kim, H.-K.; Park, J.-A.; Nam, K. S.; Lee, G. H.; Chang, Y.; Kim, T.-J. *ACS Med. Chem. Lett.* **2012**, *3*, 1003.
 22. Planchamp, C.; Montet, X.; Frossard, J. L.; Quadri, R.; Stieger, B.; Meier, P. J.; Ivancevic, M. K.; Vallee, J. P.; Terrier, F.; Pastor, C. M. *Invest. Radiol.* **2005**, *40*, 187.
 23. Van Montfoort, J. E.; Stieger, B.; Meijer, D. K. F.; Weinmann, H. J.; Meier, P. J.; Fattinger, K. E. *J. Pharmacol. Exp. Ther.* **1999**, *290*, 153.
 24. Pascolo, L.; Cupelli, F.; Anelli, P. L.; Lorusso, V.; Visigalli, M.; Uggeri, F.; Tiribelli, C. *Biochem. Biophys. Res. Commun.* **1999**, *257*, 746.
-